Published in final edited form as:
J Immunol. 2010 January 1; 184(1): 442–451. doi:10.4049/jimmunol.0900870.

Marginal Zone Precursor B Cells as Cellular Agents for Type I IFN Promoted Antigen Transport in Autoimmunity[1]

John H. Wang[*], **Jun Li**[*], **Qi Wu**[*], **PingAr Yang**[*], **Rahul D. Pawar**[*], **Shutao Xie**[*], **Laura Timares**[†], **Chander Raman**[*], **David D. Chaplin**[‡], **Lu Lu**[§], **John D. Mountz**[*,¶], and **Hui-Chen Hsu**[*,2]

[*] Department of Medicine, University of Alabama at Birmingham, Birmingham, AL 30509

[†] Department of Dermatology, University of Alabama at Birmingham, Birmingham, AL 30509

[‡] Department of Microbiology, University of Alabama at Birmingham, Birmingham, AL 30509

[§] Department of Anatomy and Neurobiology, University of Tennessee Health Science Center, Memphis, TN 38163

[¶] Birmingham VA Medical Center 35233

Abstract

The pathogenic connection of type I interferon (IFN) and its role in regulating the migration response of antigen (Ag)-delivery by B cells into lymphoid follicles in an autoimmune condition has not been well-identified. Here, we show that there was a significantly larger population of marginal zone precursor (MZ-P) B cells, defined as being $IgM^{hi}CD1d^{hi}CD21^{hi}CD23^{hi}$ in the spleens of autoimmune BXD2 mice compared to B6 mice. MZ-P B cells were highly proliferative compared to marginal zone (MZ) and follicular (FO) B cells. The intra-follicular accumulation of MZ-P B cells in proximity to germinal centers (GCs) in BXD2 mice facilitates rapid Ag delivery to the GC area, whereas Ag-carrying MZ B cells, residing predominantly in the periphery, had a lower ability to carry an Ag into the GCs. IFNα, generated by plasmacytoid dendritic cells, induced the expression of CD69 and suppressed the sphingosine-1-phosphate–induced chemotactic response, promoting FO-oriented Ag transport by MZ-P B cells. Knockout of type I IFN receptor in BXD2 (BXD2-*Ifnαr*$^{-/-}$) mice substantially diffused the intra-follicular MZ-P B cell conglomeration and shifted their location to the FO-MZ border near the marginal sinus, making Ag delivery to the FO interior less efficient. The development of spontaneous GCs was decreased in BXD2-*Ifnαr*$^{-/-}$ mice. Together, our results suggest that the MZ-P B cells are major Ag-delivery B cells and that the follicular entry of these B cells is highly regulated by type I IFN producing pDCs in the marginal sinus in the spleens of autoimmune BXD2 mice.

[1]Funding for this research was made possible by a grant from the American College of Rheumatology Research and Education Foundation *Within Our Reach: Finding a Cure for Rheumatoid Arthritis* campaign (J.D.M.), the Alliance for Lupus Research – Target Identification in Lupus program (J.D.M.), VA Merit Review Grants (1I01BX000600-01)(J.D.M.), Daiichi-Sankyo Co., Ltd. (J.D.M.), NIH (1AI 071110-01A2, 1AI 071110-02, and ARRA 3RO1AI71110-02S1) (J.D.M.), the UAB Skin Diseases Research Center (P30 AR050948-059001)(LT), and the Arthritis Investigator Award supported by the Arthritis Foundation (H.-C.H).

2Address correspondence and reprint requests to Dr. Hui-Chen Hsu, Department of Medicine, The University of Alabama at Birmingham, 1825 University Blvd, SHELB 311, Birmingham, Alabama 35294, U.S.A. Telephone: (205) 934-8909; Fax: (205) 996-6788; rheu078@uab.edu.

The localization of B cells in appropriate microenvironments of secondary lymphoid organs plays an important role in determining the fate of B cell immunity. Specifically, the B cell migration pattern into the follicular regions of the spleen can alter the tempo and frequency of T-B cell contact and thus has been proposed as one mechanism to regulate the development of autoreactive B cells (1,2). Early studies by Cyster *et al* (3) showed that under conditions of clonal selection, anergic B cells failed to enter the follicular areas, instead arresting at the T-B cell boundary in a process known as follicular exclusion. Follicular exclusion has been proposed as one B cell checkpoint mechanism to prevent B cell tolerance loss (4). Although chemokines and chemokine receptors have been paramount in shaping B cell migration patterns, we and others have shown that local cytokine production can provide additional signals to regulate the migration and retention of B cells in the follicles (5–7). In autoimmune murine models, B cells can act as Ag presenting cells (APC) and/or Ag-delivery cells to promote the development of spontaneous autoreactive germinal centers (GCs) (8–12). Treatment of autoimmune disease with B cell depletion therapy depletes B cells that mainly serve as APCs or Ag delivery cells (9,13–15).

The BXD2 mouse strain is one of the approximately 20 BXD recombinant inbred strains we have analyzed for development of autoimmune disease, including the development of features resembling human SLE and RA (16). Development of highly mutated multi-reactive autoantibodies that can induce kidney and joint disease is one of the important pathogenic features of the BXD2 mice (16,17). We have found that the BXD2 mice spontaneously form GCs in the spleens and that the expression of the gene encoding activation-induced cytidine deaminase (*Aicda*) in the GC B cells can be stimulated by activated $CD4^+$ T cells from BXD2 mice (18). There is an abundance of T_H-17 cells in the follicles and GC area. The high levels of IL-17 produced by these cells is associated with upregulation of regulator of G-protein signaling (*Rgs*)13 and *Rgs16*, and the migration arrest of B cells in response to follicular- and GC-oriented chemokines, CXCL12 and CXCL13, enabling them to form stable T-B cell conjugates and facilitate GC formation in the spleens of BXD2 mice (6).

The importance of IFNα in the spontaneous development of autoantibodies and immune complex deposition in the glomeruli has been demonstrated using murine models of lupus (19–21). Clues to the possible role of IFNα in the production of high-affinity autoantibodies can be derived from their normal physiologic mechanisms of action. IFNα has been shown to promote antibody class-switch recombination (CSR) and plasma cell differentiation under non-autoimmune conditions (22,23). To determine the reason for the coexistence of high levels of IFNα and IL-17 in the spleens of BXD2 mice, we observed that there was a significantly increased $IgM^{hi}CD1d^{hi}CD21^{hi}CD23^{hi}$ B cell population in the spleens of BXD2 mice. B cells with this phenotype are referred to as MZ-precursor (MZ-P) B cells in mice (24,25). We have further identified that the entry of MZ-P into the follicular (FO) region is promoted by IFNα, which is primarily produced by pDCs that are localized in the marginal sinus (MS). Abrogation of IFNαR in BXD2 mice attenuated the development of spontaneous GCs and autoimmune disease. Importantly, injection of BXD2 and BXD2-*Ifnαr*$^{-/-}$ mice with TNP-Ficoll demonstrated a novel finding that MZ-P B cells serve as the major Ag transporting B cells that directly deliver TNP into the GCs. Deficiency of IFNα abrogated this response. Our results suggest that follicular entry of Ag delivery MZ-P B cells facilitated by INFα may be an important mechanism to promote the autoimmune response in BXD2 mice.

Materials and Methods

Mice

Female homozygous C57BL/6 and BXD2 recombinant inbred were obtained from the Jackson Laboratory (Bar Harbor, Maine); B6-*Ifnαr*$^{-/-}$ mice were obtained from Dr. Jocelyn Demengeot at the Instituto Gulbenkian de Ciência in Oeiras, Portugal). B6-*Ifnαr*$^{-/-}$ mice were

backcrossed with BXD2 mice for seven generations, using a marker-assisted speed congenic approach with 146 markers. All mice were housed in the University of Alabama at Birmingham (UAB) Mouse Facility under specific pathogen–free conditions in a room equipped with an air-filtering system. The cages, bedding, water and food were sterilized. All mouse procedures were approved by The UAB Institutional Animal Care and Use Committee.

Flow cytometry analysis and cell sorting

Flow cytometry was performed on fluorescently-labeled single cell suspensions derived from spleens using the method we described previously (6,18). For the detection of various cell types, including pDCs and B cells, fluorescent –conjugated anti-PDCA1 (eBioscience, San Diego, CA), anti-CD19 (Biolegend, San Diego, CA), anti-IgM (Southern Biotech, Birmingham, AL), anti-CD21/35 (Biolegend), anti-CD23 (Biolegend), and anti-CD93/AA4 antibodies were employed. For the detection of CD69, CD80, and CD86, fluorescent-conjugated anti-CD69 (Biolegend), anti-CD80 (Biolegend), and anti-CD86 antibody (Biolegend) was employed. For the detection of TNP, biotinylated anti-TNP (BD Biosciences, San Jose, CA) was employed followed by utilizing fluorochrome-conjugated streptavidin. For the labeling and isolation of pDCs, all spleens were cut and treated with collagenase D (2 mg/mL) for 30 minutes at 37°C/5% CO_2 before obtaining single cell suspensions for antibody labeling. For intracellular detection of IFNα, cells were first permeabilized (BD Biosciences Cytofix/cytoperm), washed (BD Biosciences Perm/Wash), then incubated with a 1-to-1 mixture of anti-IFNα antibodies (clones RMMA-1 and F18). Cells (100,000/sample) were washed twice with FACS buffer and fixed in 1% paraformaldehyde/FACS® solution before analysis by flow cytometry using a BD-LSR-II Flow Cytometer ® (Becton Dickenson). The analysis was performed using FlowJo Software (Tree Star, Inc, Ashland, OR). Forward-angle light scatter (FSC) was used to exclude dead and aggregated cells. Some results are presented as fluorescence histograms with the relative number of cells on a linear scale versus the relative fluorescence intensity on a log scale. Acquisition and gating of FO, MZ, and MZ-P B cells was carried out based on the method described by Allman and Pillai (24). FO B cells were defined as $CD23^{hi}$ $sIgM^{lo+hi}$ $sIgD^{hi}$ $CD21^{int}$ $CD1d^{lo}$ $CD19^{+}$ cells; MZ B cells were defined as $CD23^{null+lo}$ $sIgM^{hi}$ $sIgD^{lo}$ $CD21^{hi}$ $CD1d^{hi}$ $CD19^{+}$ cells; MZ-P B cells were defined as $CD23^{hi}$ $sIgM^{hi}$ $sIgD^{hi}$ $CD21^{hi}$ $CD1d^{hi}$ $CD19^{+}$ cells. All gatings were set up to ensure that the percent of each sub-population of B cells obtained from normal B6 mice was equivalent to the previously reported results (24).

For cell sorting to isolate the different B cell populations, anti-CD19 microbeads (Miltenyi Biotec, Auburn, CA) were used to isolate whole B cells. Subsequently, the single-splenic B cell preparation was labeled with fluorescent conjugated Abs and sorted into FO, MZ, and MZ-P B cells based on the expression of CD21, CD23, and IgM, as described above. Sorting was carried out using a BD FACS Aria Cell Sorter (BD Biosciences). All sorting for pDCs was completed by positive selection using anti-PDCA1 microbeads (Miltenyi Biotech).

Immunofluorescent staining and confocal image analysis

Spleens from mice were collected, embedded in Frozen Tissue Media (Fisher Scientific) and snap-frozen in 2-methylbutane. Frozen sections (8 um thick) were dried in air for 30 minutes and fixed in acetone for 15 minutes prior to rehydration with 1% BSA for 10 min. The sections were blocked with 10% horse serum for 30 minutes at room temperature and then stained for 30 minutes at room temperature with various antibodies. The following primary antibodies conjugated to the Alexa flour dyes were used to stain spleen tissues for confocal image analysis: biotin-PNA (Vector Laboratory Inc, Burlingame, CA) to Alexa 350–streptavidin (Invitrogen, Carlsbad, CA); PNA to Alexa 350; anti–mouse CD35 (clone 8C12, BD Bioscience) to Alexa 488; anti-IgM to Alexa 555; anti-CD4 (RM4-5, Invitrogen) to Alexa 488 or 647, anti-CD23 (B3B4) to Alex488, and anti-PDCA1 to Alexa 647. For the detection of CD1d antigen, tissue

was incubated with anti-CD1d rat IgG (Biolegend) followed by anti-rat IgG conjugated to Alexa 555 (Invitrogen), after which, tissue was incubated with 10% normal rat serum at room temperature for 30 min. After 10% normal rat serum treatment, the tissues were stained with the other antibodies. For detection of TNP, anti-TNP hamster IgG (BD Sciences) incubation was followed by biotinylated anti-hamster IgG (Biolegend) incubation, and fluorochrome conjugated-streptavidin treatment. The sections were mounted in Fluormount G (Southern Biotechnology) and viewed with a Leica DM IRBE inverted Nomarski/epifluorescence microscope outfitted with LeicaTCS NT laser confocal optics (Leica Microsystems Inc, Bannockburn, IL). *In situ* quantitation of the PNA^+ GC response and TNP^+ cells was carried out using the Olympus DP2-BSW software (Olympus America, Center Velley, CA) according to the method we previously described (6).

Cell cultures

Cells, including pDCs and B cell subpopulations, were cultured with RPMI 1640 medium (Invitrogen) supplemented with 2 mM L-glutamine, 25 mM HEPES, 100 U/ml of penicillin, 100 μg/ml of streptomycin, 5.5×10^{-5} M 2-mercaptoethanol and 10% FCS, for all *in vitro* experiments.

IFNα stimulations and measurements

For CD69 expression on different B cell subpopulations in response to IFNα under *in vitro* conditions, single spleen cells were cultured in 96-well (Costar, Cambridge, MA) tissue-culture plate at 37°C/5% CO_2 in triplicate wells (1×10^4 cells per well) and stimulated with IFNα (20 ng/mL) for 12 hours. To measure IFNα levels produced by pDCs, single-cell suspensions were prepared by collagenase D (2 mg/mL) digestion of spleen tissues for 30 minutes at 37°C/5% CO_2 before sorting for pDCs. Enriched pDCs were subsequently cultured in 96-well (Costar) tissue-culture plate at 37°C/5% CO_2 in triplicate wells (1×10^4 cells per well) and stimulated with medium only, CpG (3 μM), or CpG (3 μM):DOTAP-complex (Hoffmann-La Roche Ltd). After 24 hours, culture supernatants were collected and IFNα levels were measured by ELISA (PBL Biomedical Sciences). CpG:DOTAP preparation for *in vitro* culture was formulated by mixing 19.2 μg (3 nmole) of CpG in 120 μl of PBS with 30 μl of DOTAP, incubating for 15 min, and then diluting with 850 μl of medium to make 3 μM CpG:DOTAP solution. For *in vivo* measurements of IFNα, 5 μg of CpG was administered intravenously into each mouse tail vein. 5 μg of CpG was mixed with 50 μL of PBS, while in another reaction tube, 30 μL of DOTAP was mixed with 70 μL of PBS. The CpG solution was then mixed with the DOTAP solution, incubated at room temperature for 15 minutes prior to administration. Serum levels of IFNα in each mouse were measured 4 hours later.

Cell migration assay

Single-cell suspensions of anti-CD19 MACS column (Miltenyi Biotech)-purified spleen B cells from B6, BXD2 or BXD2-*Ifnαr*$^{-/-}$ mice were stimulated with either medium only control or mouse recombinant IFNα (20 ng/ml, R&D Systems, Minneapolis, MN) for 6 hours. The cell migration assay was carried out using the protocol described by Moratz and Kehrl (26) The stimulated cells were loaded (2×10^6) into the upper well insert (5-μm pore size) of a Transwell system (5 μm pore size, Costar), and S1P was added into the bottom chamber at a final concentration of 20 nM. After incubation for 2 h at 37°C in a 5% CO_2 incubator, the migrated cells were harvested and resuspended in 300 μl FACS buffer. The cells that remained in the inserts or migrated to the lower chamber were counted using a flow cytometer, and the distribution of the subsets of $CD19^+$ B cells into migrated versus non-migrated cells was determined. The chemotaxis index was calculated by dividing the number of cells that migrated in response to chemokines by the number of cells that migrated in the absence of chemokine.

Isolation and quality control of RNA

RNA was isolated from 0.2 to 10 × 10^6 cells using the Trizol reagent (Invitrogen) or <0.2 × 10^6 using the PicoPure RNA Isolation Kit (Molecular Devices, Sunnyvale, CA). The quality of the isolated RNA was determined using an Experion Automated Electrophoresis System (Bio-Rad, Hercules, CA). RNAs that exhibited an 18S/28S ratio >1.8 were then converted to cDNA using the First Strand cDNA Synthesis Kit (Fermentas, Inc, Glen Burnie, MD).

Quantitative real-time PCR (QRT-PCR)

The expression of *Aicda*, *S1p1*, and *S1p3*, SYBR was analyzed using a quantitative real-time PCR (QRT-PCR) method. Briefly, the QRT-PCR mixtures contained Green PCR Master Mix (Bio-Rad) with the following primers: *Aicda* forward: GCCACCTTCGCAACAAGTCT; *Aicda* reverse: CCGGGCACAGTCATAGCAC (137 bp); *S1p1* forward: TGCTGTAACTGAAGGCTCAC; *S1p1* reverse GGATGCTAGTGGACACCATAG (108 bp); *S1p3* forward: CCGTAGTGATTGTGGTGAGTG; *S1p3* reverse: GGACAGCCAGCATGATGAAC; *Cdca3* forward: GAGTAGCAGACCCTCGTTCAC; *Cdca3* reverse: TCTCTACCTGAATAGGAGTGCG; *Cdca5* forward: GGACTTCACTTACTAAGCCTTC; *Cdca5* reverse: GACATCTGGGACCTCTACTG; *Cdca8* forward: ACAAGGAAGAGGCAGAAG; *Cdca8* reverse: CCGTTGATGGAGATGTTG; *Gapdh* forward: AGGTCGGTGTGAACGGATTTG; *Gapdh* reverse: TGTAGACCATGTAGTTGAGGTCA (136 bp). A final volume of 25 μl was used for QRT-PCR in an IQ5™ thermocycler (Bio-Rad). Amplification conditions were 95 °C for 3 min, followed by 40 cycles of 95 °C for 15 s and annealing for 30 s. The annealing temperature used was 54°C for *Cdca8*, 56°C for *Gapdh*, 57°C for *S1p3*, 58°C for *Aicda*, *Cdca3*, *Cdca5*, and 60°C for *S1p1* and *S1p3*.

QRT-PCR products were normalized relative to that of *Gapdh* to correct for potential differences in template input in order to determine relative mRNA levels. Results are expressed as fold differences in expression of the indicated gene relative to the expression of *Gapdh*. Standard curves were generated for every target using six 4-fold serial dilutions.

TNP-Ficoll

To specify cellular agents for antigen transport, 50 μg of TNP-Ficoll (Biosearch Technologies, Novato, CA) was intravenously administered into each mouse, and sacrificed at the indicated time points. A portion of the spleen was snap-frozen in 2-methylbutane for histological analysis, as described above. Another portion of the spleen was made into single-cell suspension and labeled for detection of TNP as described above.

Statistical analysis

All results were shown as mean ± standard error of the mean (SEM). A two-tail *t* test was used when two groups were compared for statistical differences. ANOVA test was used when more than 2 groups were compared for statistical differences. The distribution differences of MZ and MZ-P in the anatomical MZ area versus those in the anatomical follicular area between different strains of mice was tested using a chi-square test. *P* values less than 0.05 were considered significant

Results

Increased IFN-α production by plasmacytoid dendritic cells (pDCs) localized to the marginal periphery of B cell follicles in BXD2 mice

The type I IFNs, including IFNα, are highly associated with the presence of several human autoimmune diseases (20,27,28), and as demonstrated by murine models of lupus, is a causative

factor for the onset of disease (21,29). A specialized subset of dendritic cells, the pDCs, were found to efficiently generate massive amounts of type I IFNs (30). Because of the unique lupus and arthritis features developed by BXD2 mice, we questioned if high numbers of IFNα-producing pDCs are present in these mice. Flow cytometry analysis indicated that there was a significantly higher percentage of IFNα-producing pDCs in the spleens of BXD2 mice compared to the spleens of B6 mice (Fig. 1A). On gating on the IFNα producing cells, we found that the pDCs are the primary IFNα-producing cells in the spleens of BXD2 mice (Fig. 1B), which is consistent with previous reports that pDCs are efficient producers of type I IFNs (30–34). Stimulation of pDCs by type A CpG, a toll-like receptor 9 ligand, can elicit the expression and secretion of IFN-α (30,33). We found that pDCs isolated from the spleens of BXD2 mice were more responsive to *in vitro* stimulation with either type A CpG or type A CpG:DOTAP and produced significantly greater amounts of IFNα in response to these agents than equivalent numbers of pDCs isolated from the spleens of B6 mice (Fig. 1C). Immunofluorescent imaging of spleen sections of B6 mice show that there were low numbers of pDCs (green) that form a single layer surrounding non-reactive follicles (Fig. 1D). In the spleens of wild-type naïve BXD2 mice, there were large follicles with active PNA^+ GCs (blue). Surrounding these active GCs, there were increased numbers of pDCs (green) that were located away from the GCs but were primarily in the marginal periphery of the follicles in proximity to the marginal sinus (Fig. 1D).

GC formation is partially diminished BXD2-Ifnαr$^{-/-}$ mice

To determine the role of type I IFN in GC formation, the presence of GCs in wild-type BXD2 and age matched BXD2-*Ifnαr*$^{-/-}$ mice was compared. Confocal microscopy analysis of frozen spleen sections confirmed the presence of well-formed PNA^+ GCs (PNA^+; blue) located close to the central areas of follicles in 3-mo-old wild-type BXD2 mice. In age-matched BXD2-*Ifnαr*$^{-/-}$ mice, there were fewer PNA^+ GCs and those PNA^+ GCs that were present were smaller (Fig. 2A). Quantification of the number of PNA^+ follicles confirmed that there was a lower number of PNA^+ GCs per section of area in the spleens of BXD2-*Ifnαr*$^{-/-}$ mice compared to wild-type (WT) BXD2 mice (Fig. 2B) and flow cytometry indicated that BXD2 mice exhibited a higher frequency of PNA^+Fas^+ GC B cells than BXD2-*Ifnαr*$^{-/-}$ mice (Fig. 2C). This decreased formation of GCs in BXD2-*Ifnαr* $^{-/-}$ mice was associated with significantly reduced levels of *Aicda* transcripts, which encode the activation-induced cytidine deaminase (AID) protein required for class-switch recombination and somatic hypermutation, in B cells enriched from the spleens of BXD2 mice (Fig. 2D).

Increased IgM^{hi}CD21^{hi}CD23^{hi} B cells in BXD2 mice

The presence of pDCs in the marginal periphery of follicles suggests that type I IFNs can signal B cells in the MZ and B cells that traffic near the border region between the MZ and FO. We have shown previously that the percentage of MZ B cells, defined by their anatomic location in the MZ, and as exhibiting the CD21^{hi} CD23^{lo} phenotype, is lower in the spleens of BXD2 mice than age-matched B6 mice whereas the percentage of FO B cells is higher (6). To determine whether this reduction in mature MZ B cells in BXD2 mice is due to a lack of precursor or altered B cell development under the influence of pDCs in the marginal sinus, we analyzed the phenotype of B cells in B6, BXD2 and BXD2-*Ifnαr*$^{-/-}$ mice. The relative expression of CD23 on the MZ B cells subdivides these cells into two functionally different populations (24,25,35,36). The CD23^{lo}IgM^{hi}CD21^{hi} B cells are considered to be mature MZ B cells whereas the CD23^{hi} IgM^{hi}CD21^{hi} B cells are thought to be MZ-precursor (MZ-P) (24,25,35,36).

As defined by IgM^{hi}CD21^{hi}, the highest percentage of MZ B cells was seen in B6 mice, with lower percentages in BXD2 and in BXD2-*Ifnαr*$^{-/-}$ mice (Fig. 3A). However, the majority of the IgM^{hi}CD21^{hi} MZ B cells from the spleens of BXD2 mice exhibited the CD23^{hi} MZ-P

phenotype (Fig. 3B, ***middle panel***), which was significantly greater compared to B6 mice, in which the majority of IgM^{hi}CD21^{hi} MZ B cells exhibited the CD23^{lo} MZ phenotype (Fig. 3B, ***upper panel***). Although exhibiting a higher frequency of IgM^{hi}CD21^{hi}CD23^{hi} MZ-P B cells than in B6 mice, BXD2-*Ifnαr*$^{-/-}$ mice displayed significantly decreased percentages than their wild-type counterparts for this particular cell population (Fig. 3B, ***lower panel***).

Flow cytometry analysis for the FO, CD23^{lo} MZ, and CD23^{hi} MZ-P B cells also show that both MZ and MZ-P B cell populations express high levels of CD1d compared to the FO B cell population (Fig. 3C). The percentages of MZ and MZ-P B cell expressing CD1d are comparable, whereas FO B cells express significantly less CD1d than either of the two populations (Fig. 3D). There was no difference in the expression of IgD and CD93 (AA4) in IgM^{hi}CD21^{hi}CD23^{hi} B cells from all 3 strains of mice (IgD^{hi}CD93$^{-/lo}$, data not shown). The results suggest that these abnormally expanded B cells in BXD2 mice exhibit the characteristics as the previously described MZ-P B cells (24,25,35,36).

The total counts of IgM^{hi}CD21^{hi} MZ B cells in the spleens were higher in the wild-type BXD2 mice and in BXD2-*Ifnαr*$^{-/-}$ mice than in the B6 mice due to the significantly enlarged spleen sizes of these BXD2 mice (6)(Fig. 3E). There were fewer conventional CD23^{lo}IgM^{hi}CD21^{hi} MZ B cells, but greatly elevated CD23^{hi}IgM^{hi}CD21^{hi} MZ-P B cells, in the spleens of BXD2 mice compared to the spleens of B6 mice (Fig. 3E). Although the total spleen cell count is near equivalent between wild-type BXD2 and BXD2-*Ifnαr*$^{-/-}$ mice, there was a significantly lower percentage and lower total counts of MZ-P B cells in BXD2-*Ifnαr*$^{-/-}$ mice compared to BXD2 mice (Fig. 3E).

To determine if the percent of MZ-P B cells exhibited a correlation with the levels of IFNα in BXD2 mice, the MZ-P B cells as a percentage of IgM^{hi}CD21^{hi} B cells were calculated in 1-, 3-, and 8-mo old BXD2 mice. The results indicate that the percent of MZ-P B cells peaked in 3-mo old BXD2 mice (Supplemental Fig. 1A). Consistent with the role of type I IFN in promoting MZ-P B cells development, 3-mo old BXD2 mice exhibited the highest serum IFNα levels in response to type A CpG compared to 1- and 8-mo ages (Supplemental Fig. 1B). The lower ability of pDCs from older BXD2 mice to produce type I IFN appears to be associated with their maturation status as increased in the expression of CD80 and CD86 are observed in pDCs from 8-mo-old BXD2 mice (Supplemental Fig. 1C).

Compared with FO and CD23^{lo} MZ B cells, MZ-P B cells from BXD2 mice exhibited the highest proliferative response after anti-CD40 and anti-IgM stimulation (Supplemental Fig. 2A, 2B). *In vivo*, MZ-P B cells also exhibited the highest expression of genes involved in cell division, including *Cdca3*, *Cdca5*, and *Cdca8*, compared to either MZ or FO B cells (Supplemental Fig. 2C). BXD2 MZ-P B cells exhibited higher message levels of these proliferation genes than B6 MZ-P B cells, demonstrating the unique hyper-proliferation phenotype of this B cell subpopulation in BXD2 mice.

Increased counts and intra-follicular concentration of MZ-P B cells in proximity to GCs in type I IFN signaling-competent wild-type BXD2 mice

MZ B cells can be distinguished by their phenotype (CD21^{hi}IgM^{hi}CD23^{lo}) and their location outside of the marginal sinus. This location enables them to encounter blood-borne IgM-immune complexes (37). In contrast, the location of MZ-P B cells is less well established. Compared to FO (CD1d^{lo}CD23^{hi}) and MZ (CD1d^{hi}CD23^{lo}), only MZ-P B cells exhibit the CD1d^{hi}CD23^{hi} phenotype, we therefore used anti-CD1d and anti-CD23 staining to determine the location of the MZ-P B cells in the spleens of the B6, BXD2, and BXD2-*Ifnαr*$^{-/-}$ mice (Fig 4A–F). As expected, CD1d^{hi}CD23^{lo} MZ B cells (green) surround the B cell follicle in proximity to the marginal sinus in the spleens of all three strains of mice (Fig 4A–C). In the spleens of BXD2 mice, there is an area of CD1d^{hi} B cells that are also CD23^{hi} near the GCs

(yellow) (Fig. 4B, 4E). These CD1d^{hi}CD23^{hi} B cells are situated adjacent to a GC and opposite to the CD4^{+} T-cell area, suggesting that these CD1d^{hi}CD23^{hi} B cells are located near the light zone of a GC (38,39). In contrast, significantly decreased numbers of MZ-P B cells appear to distribute diffusely within the B cell follicles of B6 mice (Fig. 4A, 4D). Similarly, in the absence of type I IFN signaling in BXD2-*Ifnαr*$^{-/-}$ mice, there were low numbers of MZ-P B cells that are distributed diffusely, many of which are near the FO-MZ border of the FO. There was an absence of concentrated clusters of MZ-P B cells that are present in BXD2-*Ifnαr*$^{-/-}$ spleens (Fig. 4C, 4F), even in the presence of a developing GC in BXD2-*Ifnαr*$^{-/-}$ mice (Fig. 4F).

Quantitative analysis by counting the number of CD1d^{hi}CD23^{lo} MZ B cells per visual field showed that the greater majority of MZ B cells reside in the MZ (Fig. 4G, **open area),** while a minor fraction is located in the FO (Fig. 4G, solid area). In contrast, the majority of CD1d^{hi}CD23^{hi} MZ-P B cells reside in the FO in the spleens of BXD2 mice (Fig. 4H, solid area). A chi-square test analysis indicates a significantly greater percentage of MZ-P B cells residing in the FO relative to the MZ in the spleens of wild-type BXD2 mice than in the spleens of either B6 or BXD2-*Ifnαr*$^{-/-}$ mice (Fig. 4H), whereas no significant differences were observed for the residence of MZ B cells among the B6, BXD2, and BXD2-*Ifnαr*$^{-/-}$ mice (Fig. 4G).

Type I IFN signaling induces and maintains higher CD69 surface expression and lowers S1p1 message levels by MZ-P B cells in BXD2 mice

S1P$_1$ surface expression is known to antagonize the surface expression of CD69 (40), and its expression on B cells is known to promote their localization to the MZ (41). Because greater fractions of MZ-P B cells are geographically localized within the FO in the BXD2 mice than those in the B6 or BXD2-*Ifnαr*$^{-/-}$ mice (Fig. 4H), we sought to determine the expression of CD69 and *S1p1*. The highest surface expression of CD69 was observed on freshly isolated MZ-P B cells compared to MZ and FO B cells (Fig. 5A). CD69 surface expression on MZ and MZ-P B cells was decreased in BXD2-*Ifnαr*$^{-/-}$ mice compared with their wild-type counterparts (Fig. 5A). The percentage of CD69^{+}IgM^{hi}CD21^{hi}CD23^{hi} MZ-P B cells was significantly greater compared to either of the other two CD69^{+} B cell populations in BXD2 mice (Fig. 5B). In contrast, MZ-P B cells from BXD2-*Ifnαr*$^{-/-}$ mice exhibited significantly suppressed levels of CD69 (Fig. 5B).

To further test whether type I IFNs can increase the surface expression of CD69 on the individual B cell populations, cell-sorted FO, MZ, and MZ-P B cells were stimulated with IFNα *in vitro*. Culture with IFNα led to significant induction of CD69 surface expression on all three B cell populations from BXD2 mice (Fig, 5C). More importantly, IFNα significantly increased CD69 surface expression on MZ-P B cells to a greater level than either FO or MZ B cells in BXD2 mice, indicating MZ-P B cells have a greater sensitivity to IFNα (Fig. 5D). In contrast, CD69 surface expression on MZ-P B cells from BXD2-*Ifnαr*$^{-/-}$ mice remained significantly suppressed (Fig. 5D).

Consistent with the higher percentage of MZ-P B cells from BXD2 mice that expressed CD69, the cell-sorted MZ-P B cells expressed lower levels of *S1p1* transcripts when compared to the CD23^{lo} MZ B cells from these mice (Fig. 5E). In contrast, MZ B cells displayed comparable levels of *S1p1* transcripts (Fig. 5E), regardless of whether type I IFN signaling is present or not. Furthermore, *S1p3* transcript levels were significantly suppressed in MZ-P B cells independent of type I IFN signaling (Fig. 5E). Analysis of the chemotactic response towards S1P *in vitro* indicated that the migration of the MZ B cell in response to S1P was equivalent between BXD2 and BXD2-*Ifnαr*$^{-/-}$ mice (Fig. 5F). However, the S1P-induced chemoattractive effect on MZ-P B cells from the BXD2 mice was lower than that of MZ-P cells from BXD2-*Ifnαr*$^{-/-}$ mice (Fig. 5F). Consistent with the elevated expression of CD69 on the BXD2 MZ-P cells, *in vitro* IFNα stimulation of B cells from BXD2 mice led to further

reduction of the chemotactic response toward S1P, especially in the $CD23^{hi}$ MZ-P B cell population, and this decrease was not observed in B cells isolated from BXD2-*Ifnαr*$^{-/-}$ mice (Fig. 5F). Together, these results suggest a mechanistic model in which the production of type I IFNs, including IFNα, by pDCs localized to the marginal periphery of B cell follicles in BXD2 spleens can upregulate the surface expression of CD69 on MZ-P B cells to induce intra-follicular aggregations that may collectively facilitate germinal center induction.

Type I IFNs promoted antigen-delivery to GCs by MZ-P B cells in BXD2 mice

One critical function of B-cell migration into the follicular and GC region is to serve as antigen-delivery cells (42). In order to determine if MZ-P B cells could transport Ag and be influenced by type I IFNs, BXD2 and BXD2-*Ifnαr*$^{-/-}$ mice were analyzed at 1 hour after TNP-Ficoll administration. TNP-Ficoll has been shown to bind to MZ B cells via a complement receptor (CD21-CD35) dependent manner. This facilitates the visualization of the shuffling of TNP capturing $CD21^{+}$ B cells (43,44). Since both MZ and MZ-P B cell express high levels of CD21, we determined if MZ and MZ-P B cells exhibit an equivalent ability to bind to and deliver TNP-Ficoll into the follicles. Flow cytometry analysis indicated that there was near equivalent binding of TNP-Ficoll to MZ and MZ-P B cells from either BXD2 or BXD2-*Ifnαr*$^{-/-}$ mice, which were significantly higher than TNP-Ficoll binding to $CD21^{lo}$ FO B cells (Fig. 6A, 6B). However, histological analysis revealed substantial accumulation of TNP-Ficoll carried by MZ-P B cells in proximity to the GCs in BXD2 mice. A representative GC is shown and is adjacent to concentrations of TNP^{+} MZ-P B cells (dark blue) (Fig. 6C). While MZ B cells could trap TNP-Ficoll, the greater majority of TNP^{+}MZ B cells (light pink) were located in the MZ, and not adjacent to the developing GC (Fig. 6D, 6G). Consistent with the earlier observation that MZ-P B cells have a diffuse geographical distribution and a preference for locations near the FO-MZ border in the spleens from BXD2-*Ifnαr*$^{-/-}$ mice (Fig. 6E), we did not observe significant aggregates of TNP^{+}MZ-P B cells inside the B cell follicle. Rather, many of the TNP^{+}MZ-P B cells remained near the FO-MZ border in proximity to the marginal sinus (Fig. 6F). The average number of MZ-P TNP^{+} B cells in the follicle is 74±6 in BXD2 mice, compared to only 16±4 in BXD2-*Ifnar*$^{-/-}$ mice (Fig. 6G). This result shows that MZ-P B cells are especially capable of carrying antigen into the follicle in BXD2 mice that have intact IFNαR signal.

Discussion

We have established previously that BXD2 mice spontaneously develop high levels of circulating high-affinity nephritogenic and arthrogenic pathogenic autoantibodies and that the spontaneous formation of GCs in the spleen is critical to the production of these high-affinity pathogenic autoantibodies (16–18). In the present study, we show that there are increased counts of pDCs in the spleens of BXD2 mice. These pDCs exhibit significantly elevated expression of IFNα and are the primary producers of this cytokine. We further showed that type I IFNs play a role in the development of lupus in the BXD2 mice by demonstrating that a deficiency of the IFNαR in these mice leads to a reduction in the spontaneous formation of GCs. Strikingly, although the type I IFN signature and the expanded development of T_H-17 cells both have been reported to be associated with lupus in humans (45–47), IFNα by itself has been found to suppress T_H-17 development (48). Because IFNα is mainly produced by pDCs which are located in the MZ and we have shown previously showed that T_H-17 cells are preferentially located in the inner follicle or inside of a GC (6), our results therefore suggest that spatial compartmentalization of IFNα producing pDCs and IL-17 producing CD4 T cells in the BXD2 spleens is one mechanism to enable the cooperative effects of these two cytokines.

In the spleens of naïve mice, pDCs are scattered mainly in the T cell area and in the red pulp, and are only rarely found in the MZ (49); however, upon infection with virus, or after CpG

stimulation, pDCs migrate to the MZ area and produce IFNα within the first 36 hours of exposure (49), suggesting that the relocation of pDCs into the MZ area and production of IFNα in this area is part of an early host defense mechanism (49). Our observations suggest that the location of IFNα-producing pDCs in the MZ region serves to act on the immediate cells in their vicinity, including those in the MZ and the FO regions in near proximity, to affect a chain of events that lead to GC induction and maintenance.

BXD2 mice, unlike their B6 counterparts, display an elevated percentage and count of MZ-P B cells, by which the majority of $IgM^{hi}CD21^{hi}$ B cells are $CD23^{hi}$, rather than $CD23^{lo}$. Compared with normal B6 MZ-P B cells, MZ-P B cells from BXD2 mice exhibited dramatically elevated proliferative response by anti-IgM and anti-CD40 stimulation. Consistent with these *in vitro* observations, MZ-P B cells directly isolated from BXD2 mice demonstrated higher levels of cell cycle and cell division cycle associated genes than either FO or MZ B cells, and MZ-P B cells from B6 mice. Among these, proteins encoded by *Cdca3* (Tome-1), and *Cdca8* (Borea) are important regulators of mitosis (50,51). Protein encoded by *Cdca5* (Sororin) is required for sister chromatid cohesion (52). The hyper-proliferative phenotype of MZ-P B cells from BXD2 mice may account for the larger percentage of these cells in the spleens of these mice.

Interestingly, BXD2-*Ifnαr*$^{-/-}$ mice display decreased numbers of MZ-P B cells compared to wild-type BXD2 mice. Type I IFN receptor deletion shifts the migration pattern of MZ-P B cells towards the FO-MZ border away from the FO interior and GCs, possibly facilitating the migration of MZ-P B cells to the MZ and becoming permanently MZ B cells in response to the chemical milieu in the MZ (40,53). Accordingly, BXD2-*Ifnαr*$^{-/-}$ mice exhibit decreased MZ-P B cells with a concomitant increased count of MZ B cells compared to wild-type BXD2 mice. Examining BXD2 mice at different ages, we observed peak counts of MZ-P B cells at 3 months of age. This trend correlates with the ability of pDCs to produce IFNα, which is high at 3 months of age, and becomes suppressed at 8 months of age. The down-regulation of IFNα in older BXD2 mice correlated with the increased expression of maturation markers, CD80 and CD86, on pDCs. This is consistent with the previous finding that mature pDCs express higher levels of CD80 and CD86 to make pDCs more efficient APCs but reduce their type I IFN production (33). Chronic exposure to and activation by Ags could induce the phenotypic shift in pDCs from primary interferon-producers to efficient APCs in BXD2 mice. An upward trend of serum levels of IFNα from 1 to 3-mo of age in BXD2 mice can promote MZ-P B cell expansion and their inward follicular movement to induce and maintain GCs. This is consistent with increased percentages of MZ-P B cells in BXD2 mice from 1 to 3 months of age. The finding that these occur prior to significant development of autoantibody production, which occurs at 4 to 6 months of age (17), indicates that MZ-P B cell expansion and its regulation by type I IFN is an early event prior to disease onset.

Importantly, our results suggest that type I IFNs exhibit an important effect to promote the follicular-oriented migration of MZ-P B cells. Because CD69 surface expression is diminished in FO, MZ, and MZ-P B cells from BXD2-*Ifnαr*$^{-/-}$ mice, type I IFN can regulate *S1p1* expression within each of these B cell populations. In spite of IFNα stimulation under *in vitro* conditions, CD69 surface expression in all three B cell populations in BXD2-*Ifnαr*$^{-/-}$ mice remained suppressed. Interestingly, MZ-P B cells in IFNαR intact BXD2 mice expressed the highest levels of cell surface CD69. When stimulated with IFNα, MZ-P B cells from BXD2 mice exhibited the highest surface expression of CD69 compared to either FO or MZ B cells. Consistent with the antagonistic relationship between CD69 and $S1P_1$ expression, when type I IFN receptor is deleted, *S1p* transcript levels becomes elevated. Furthermore, $S1P_3$, known to be highly expressed in MZ B cells, had significantly depressed transcript levels in the MZ-P B cells, regardless of whether type I IFN signaling is present or absent. $S1P_3$ stabilizes the positioning of B cells in the MZ (41). Its depressed levels in MZ-P B cells further suggest that,

compared to MZ, MZ-P B cells exhibit a higher tendency to migrate into the FO. We have also determined the chemotactic responses of MZ and MZ-P from both BXD2 and BXD2-*Ifnαr*$^{-/-}$ mice to CXCL12, CXCL13, CCL19 and CCL21 and found that the only chemokines that provide differentially chemoattractive effects to MZ and MZ-P B cells from these two strains is CXCL13. Both MZ and MZ-P B cells from BXD2 mice exhibited a stronger migration response towards CXCL13, compared to the same cells from BXD2-*Ifnαr*$^{-/-}$ mice (data not shown). The results therefore suggest that the dominant effects of IFNα to regulate the follicular entry of MZ-P B cells were via its suppression on the S1P chemotactic response. Potentially, pDCs residing in the MZ can generate massive amounts of IFNα to achieve this.

McHeyzer-Williams and colleagues (54) describe that during the initial phase of protein immunization, naïve B cells specifically recognize the protein Ag and transport this Ag to initiate the T cell-dependent B cell response in Checkpoint I. They further proposed that these B cells contact cell-associated Ag for priming during this early initiation phase of adaptive immunity. In parallel, naïve T helper cells expand, differentiate into effector T helper cells, and migrate to the T-B borders to contact peptide:MHC-II-expressing Ag-primed B cells in Checkpoint II. Despite this importance of B cells as the initial Ag transporting B cells in adaptive immunity, the identity and unique property of these initial Ag transporting B cells and how these B cells can affect the development of autoimmune disease are not well known (55). Our present study suggests that MZ-P B cells are the dominant B cells that transport Ag directly into a GC in BXD2 mice. In the context of autoimmunity, this continuous supply of Ag to the GCs can potentially drive and maintain the generation of autoantibody-producing plasma cells. In BXD2-*Ifnαr*$^{-/-}$ mice, however, MZ-P B cells carrying Ag are now relegated to the periphery near the FO-MZ border in proximity to the marginal sinus, and thereby prevent the influx of Ag delivery B cells to migrate into the inner follicles. The present results suggest that production of IFNα in the marginal sinus to drive the follicular migration of Ag transporting MZ-P B cells into the GC area exhibits the potential to break the closely monitored Checkpoints I and II of the T-dependent humoral responses, leading to the development of spontaneous GCs and pathogenic autoantibodies in BXD2 mice.

Supplementary Material

Refer to Web version on PubMed Central for supplementary material.

Acknowledgments

We thank Mr. Marion L. Spell of the UAB AIDS FACS Core Facility and Ms. Enid Keyser of the Arthritis and Musculoskeletal Disease Center Analytic and Preparative Cytometry Facility for operating the FACS instrument. We thank Mr. Albert Tousson of the High Resolution Imaging Facility for assistance on operating the confocal imaging equipment. We thank Dr. Jocelyn Demengeot at the Instituto Gulbenkian de Ciência in Oeiras, Portugal to provide B6-*Ifnαr*$^{-/-}$ mice. We thank Dr. Fiona Hunter for expert review of the manuscript and Ms. Carol Humber for excellent secretarial assistance.

Abbreviations in this paper

DOTAP	N-[1-(2,3-Dioleoyloxy)propyl]-N,N,Ntrimethylammonium Methylsulfate
FO	follicle or follicular
GC	germinal center
IFN	interferon
IFNαR	type I IFN receptor
MS	marginal sinus

MZ	marginal zone
MZ-P	marginal zone precursor
PDC	plasmacytoid dendritic cell
PNA	peanut agglutinin
QRT-PCR	quantitative real-time PCR
S1P	sphingosine-1-phosphate
TNP	(2,4,6-Trinitrophenyl)-Protein

References

1. Duan B, Niu H, Xu Z, Sharpe AH, Croker BP, Sobel ES, Morel L. Intrafollicular location of marginal zone/CD1d(hi) B cells is associated with autoimmune pathology in a mouse model of lupus. Lab Invest 2008;88:1008–1020. [PubMed: 18607347]
2. Paul E, Nelde A, Verschoor A, Carroll MC. Follicular exclusion of autoreactive B cells requires FcgammaRIIb. Int Immunol 2007;19:365–373. [PubMed: 17307801]
3. Cyster JG, Hartley SB, Goodnow CC. Competition for follicular niches excludes self-reactive cells from the recirculating B-cell repertoire. Nature 1994;371:389–395. [PubMed: 7522305]
4. Schmidt KN, Cyster JG. Follicular exclusion and rapid elimination of hen egg lysozyme autoantigen-binding B cells are dependent on competitor B cells, but not on T cells. J Immunol 1999;162:284–291. [PubMed: 9886397]
5. Corcione A, Ottonello L, Tortolina G, Tasso P, Ghiotto F, Airoldi I, Taborelli G, Malavasi F, Dallegri F, Pistoia V. Recombinant tumor necrosis factor enhances the locomotion of memory and naive B lymphocytes from human tonsils through the selective engagement of the type II receptor. Blood 1997;90:4493–4501. [PubMed: 9373260]
6. Hsu HC, Yang P, Wang J, Wu Q, Myers R, Chen J, Yi J, Guentert T, Tousson A, Stanus AL, Le TV, Lorenz RG, Xu H, Kolls JK, Carter RH, Chaplin DD, Williams RW, Mountz JD. Interleukin 17-producing T helper cells and interleukin 17 orchestrate autoreactive germinal center development in autoimmune BXD2 mice. Nat Immunol 2008;9:166–175. [PubMed: 18157131]
7. Moratz C V, Kang H, Druey KM, Shi CS, Scheschonka A, Murphy PM, Kozasa T, Kehrl JH. Regulator of G protein signaling 1 (RGS1) markedly impairs Gi alpha signaling responses of B lymphocytes. J Immunol 2000;164:1829–1838. [PubMed: 10657631]
8. Chan O, Shlomchik MJ. A new role for B cells in systemic autoimmunity: B cells promote spontaneous T cell activation in MRL-lpr/lpr mice. J Immunol 1998;160:51–59. [PubMed: 9551955]
9. Datta SK. Anti-CD20 antibody is an efficient therapeutic tool for the selective removal of autoreactive T cells. Nat Clin Pract Rheumatol 2009;5:80–82. [PubMed: 19092831]
10. Eisenberg R. Targeting B cells in SLE: the experience with rituximab treatment (anti-CD20). Endocr Metab Immune Disord Drug Targets 2006;6:345–350. [PubMed: 17214580]
11. Roth R, Gee RJ, Mamula MJ. B lymphocytes as autoantigen-presenting cells in the amplification of autoimmunity. Ann N Y Acad Sci 1997;815:88–104. [PubMed: 9186642]
12. Weyand CM, Goronzy JJ. Ectopic germinal center formation in rheumatoid synovitis. Ann N Y Acad Sci 2003;987:140–149. [PubMed: 12727633]
13. Bystry RS, Aluvihare V, Welch KA, Kallikourdis M, Betz AG. B cells and professional APCs recruit regulatory T cells via CCL4. Nat Immunol 2001;2:1126–1132. [PubMed: 11702067]
14. Goronzy JJ, Weyand CM. B cells as a therapeutic target in autoimmune disease. Arthritis Res Ther 2003;5:131–135. [PubMed: 12723978]
15. Kessel A, Rosner I, Toubi E. Rituximab: beyond simple B cell depletion. Clin Rev Allergy Immunol 2008;34:74–79. [PubMed: 18240027]
16. Mountz JD, Yang P, Wu Q, Zhou J, Tousson A, Fitzgerald A, Allen J, Wang X, Cartner S, Grizzle WE, Yi N, Lu L, Williams RW, Hsu HC. Genetic segregation of spontaneous erosive arthritis and

generalized autoimmune disease in the BXD2 recombinant inbred strain of mice. Scand J Immunol 2005;61:128–138. [PubMed: 15683449]

17. Hsu HC, Zhou T, Kim H, Barnes S, Yang P, Wu Q, Zhou J, Freeman BA, Luo M, Mountz JD. Production of a novel class of polyreactive pathogenic autoantibodies in BXD2 mice causes glomerulonephritis and arthritis. Arthritis Rheum 2006;54:343–355. [PubMed: 16385526]
18. Hsu HC, Wu Y, Yang P, Wu Q, Job G, Chen J, Wang J, Accavitti-Loper MA, Grizzle WE, Carter RH, Mountz JD. Overexpression of activation-induced cytidine deaminase in B cells is associated with production of highly pathogenic autoantibodies. J Immunol 2007;178:5357–5365. [PubMed: 17404321]
19. Braun D, Geraldes P, Demengeot J. Type I Interferon controls the onset and severity of autoimmune manifestations in lpr mice. J Autoimmun 2003;20:15–25. [PubMed: 12604309]
20. Koutouzov S, Mathian A, Dalloul A. Type-I interferons and systemic lupus erythematosus. Autoimmun Rev 2006;5:554–562. [PubMed: 17027892]
21. Santiago-Raber ML, Baccala R, Haraldsson KM, Choubey D, Stewart TA, Kono DH, Theofilopoulos AN. Type-I interferon receptor deficiency reduces lupus-like disease in NZB mice. J Exp Med 2003;197:777–788. [PubMed: 12642605]
22. Jego G, Palucka AK, Blanck JP, Chalouni C, Pascual V, Banchereau J. Plasmacytoid dendritic cells induce plasma cell differentiation through type I interferon and interleukin 6. Immunity 2003;19:225–234. [PubMed: 12932356]
23. Le Bon A, Schiavoni G, D'Agostino G, Gresser I, Belardelli F, Tough DF. Type i interferons potently enhance humoral immunity and can promote isotype switching by stimulating dendritic cells in vivo. Immunity 2001;14:461–470. [PubMed: 11336691]
24. Allman D, Pillai S. Peripheral B cell subsets. Curr Opin Immunol 2008;20:149–157. [PubMed: 18434123]
25. Srivastava B, Quinn WJ 3rd, Hazard K, Erikson J, Allman D. Characterization of marginal zone B cell precursors. J Exp Med 2005;202:1225–1234. [PubMed: 16260487]
26. Moratz C, Kehrl JH. In vitro and in vivo assays of B-lymphocyte migration. Methods Mol Biol 2004;271:161–171. [PubMed: 15146120]
27. Cavanagh LL, Boyce A, Smith L, Padmanabha J, Filgueira L, Pietschmann P, Thomas R. Rheumatoid arthritis synovium contains plasmacytoid dendritic cells. Arthritis Res Ther 2005;7:R230–240. [PubMed: 15743469]
28. Yao Y, Richman L, Morehouse C, de los Reyes M, Higgs BW, Boutrin A, White B, Coyle A, Krueger J, Kiener PA, Jallal B. Type I interferon: potential therapeutic target for psoriasis? PLoS One 2008;3:e2737. [PubMed: 18648529]
29. Lian ZX, Kikuchi K, Yang GX, Ansari AA, Ikehara S, Gershwin ME. Expansion of bone marrow IFN-alpha-producing dendritic cells in New Zealand Black (NZB) mice: high level expression of TLR9 and secretion of IFN-alpha in NZB bone marrow. J Immunol 2004;173:5283–5289. [PubMed: 15470074]
30. Colonna M, Trinchieri G, Liu YJ. Plasmacytoid dendritic cells in immunity. Nat Immunol 2004;5:1219–1226. [PubMed: 15549123]
31. Hanten JA, Vasilakos JP, Riter CL, Neys L, Lipson KE, Alkan SS, Birmachu W. Comparison of human B cell activation by TLR7 and TLR9 agonists. BMC Immunol 2008;9:39. [PubMed: 18652679]
32. Hughes GC, Thomas S, Li C, Kaja MK, Clark EA. Cutting edge: progesterone regulates IFN-alpha production by plasmacytoid dendritic cells. J Immunol 2008;180:2029–2033. [PubMed: 18250406]
33. Liu YJ. IPC: professional type 1 interferon-producing cells and plasmacytoid dendritic cell precursors. Annu Rev Immunol 2005;23:275–306. [PubMed: 15771572]
34. Wu P, Wu J, Liu S, Han X, Lu J, Shi Y, Wang J, Lu L, Cao X. TLR9/TLR7-triggered downregulation of BDCA2 expression on human plasmacytoid dendritic cells from healthy individuals and lupus patients. Clin Immunol 2008;129:40–48. [PubMed: 18684674]
35. Saito T, Chiba S, Ichikawa M, Kunisato A, Asai T, Shimizu K, Yamaguchi T, Yamamoto G, Seo S, Kumano K, Nakagami-Yamaguchi E, Hamada Y, Aizawa S, Hirai H. Notch2 is preferentially expressed in mature B cells and indispensable for marginal zone B lineage development. Immunity 2003;18:675–685. [PubMed: 12753744]

36. Srivastava B, Lindsley RC, Nikbakht N, Allman D. Models for peripheral B cell development and homeostasis. Semin Immunol 2005;17:175–182. [PubMed: 15826822]
37. Ferguson AR, Youd ME, Corley RB. Marginal zone B cells transport and deposit IgM-containing immune complexes onto follicular dendritic cells. Int Immunol 2004;16:1411–1422. [PubMed: 15326094]
38. Allen CD, Okada T, Cyster JG. Germinal-center organization and cellular dynamics. Immunity 2007;27:190–202. [PubMed: 17723214]
39. McHeyzer-Williams LJ, Driver DJ, McHeyzer-Williams MG. Germinal center reaction. Curr Opin Hematol 2001;8:52–59. [PubMed: 11138628]
40. Shiow LR, Rosen DB, Brdickova N, Xu Y, An J, Lanier LL, Cyster JG, Matloubian M. CD69 acts downstream of interferon-alpha/beta to inhibit S1P1 and lymphocyte egress from lymphoid organs. Nature 2006;440:540–544. [PubMed: 16525420]
41. Cinamon G, Matloubian M, Lesneski MJ, Xu Y, Low C, Lu T, Proia RL, Cyster JG. Sphingosine 1-phosphate receptor 1 promotes B cell localization in the splenic marginal zone. Nat Immunol 2004;5:713–720. [PubMed: 15184895]
42. Fazilleau N, Mark L, McHeyzer-Williams LJ, McHeyzer-Williams MG. Follicular helper T cells: lineage and location. Immunity 2009;30:324–335. [PubMed: 19303387]
43. Cinamon G, Zachariah MA, Lam OM, Foss FW Jr, Cyster JG. Follicular shuttling of marginal zone B cells facilitates antigen transport. Nat Immunol 2008;9:54–62. [PubMed: 18037889]
44. Guinamard R, Okigaki M, Schlessinger J, Ravetch JV. Absence of marginal zone B cells in Pyk-2-deficient mice defines their role in the humoral response. Nat Immunol 2000;1:31–36. [PubMed: 10881171]
45. Pernis AB. Th17 cells in rheumatoid arthritis and systemic lupus erythematosus. J Intern Med 2009;265:644–652. [PubMed: 19493058]
46. Yang J, Chu Y, Yang X, Gao D, Zhu L, Wan L, Li M. Th17 and natural Treg cell population dynamics in systemic lupus erythematosus. Arthritis Rheum 2009;60:1472–1483. [PubMed: 19404966]
47. Zhao XF, Pan HF, Yuan H, Zhang WH, Li XP, Wang GH, Wu GC, Su H, Pan FM, Li WX, Li LH, Chen GP, Ye DQ. Increased serum interleukin 17 in patients with systemic lupus erythematosus. Mol Biol Rep 2009. 2009 Apr 4;
48. Moschen AR, Geiger S, Krehan I, Kaser A, Tilg H. Interferon-alpha controls IL-17 expression in vitro and in vivo. Immunobiology 2008;213:779–787. [PubMed: 18926293]
49. Asselin-Paturel C, Brizard G, Chemin K, Boonstra A, O'Garra A, Vicari A, Trinchieri G. Type I interferon dependence of plasmacytoid dendritic cell activation and migration. J Exp Med 2005;201:1157–1167. [PubMed: 15795237]
50. Ayad NG, Rankin S, Murakami M, Jebanathirajah J, Gygi S, Kirschner MW. Tome-1, a trigger of mitotic entry, is degraded during G1 via the APC. Cell 2003;113:101–113. [PubMed: 12679038]
51. Ruchaud S, Carmena M, Earnshaw WC. The chromosomal passenger complex: one for all and all for one. Cell 2007;131:230–231. [PubMed: 17956723]
52. Schmitz J, Watrin E, Lenart P, Mechtler K, Peters JM. Sororin is required for stable binding of cohesin to chromatin and for sister chromatid cohesion in interphase. Curr Biol 2007;17:630–636. [PubMed: 17349791]
53. Rubtsov AV, Swanson CL, Troy S, Strauch P, Pelanda R, Torres RM. TLR Agonists Promote Marginal Zone B Cell Activation and Facilitate T-Dependent IgM Responses. J Immunol 2008;180:3882–3888. [PubMed: 18322196]
54. McHeyzer-Williams LJ, Pelletier N, Mark L, Fazilleau N, McHeyzer-Williams MG. Follicular helper T cells as cognate regulators of B cell immunity. Curr Opin Immunol 2009;21:266–273. [PubMed: 19502021]
55. Batista FD, Harwood NE. The who, how and where of antigen presentation to B cells. Nat Rev Immunol 2009;9:15–27. [PubMed: 19079135]

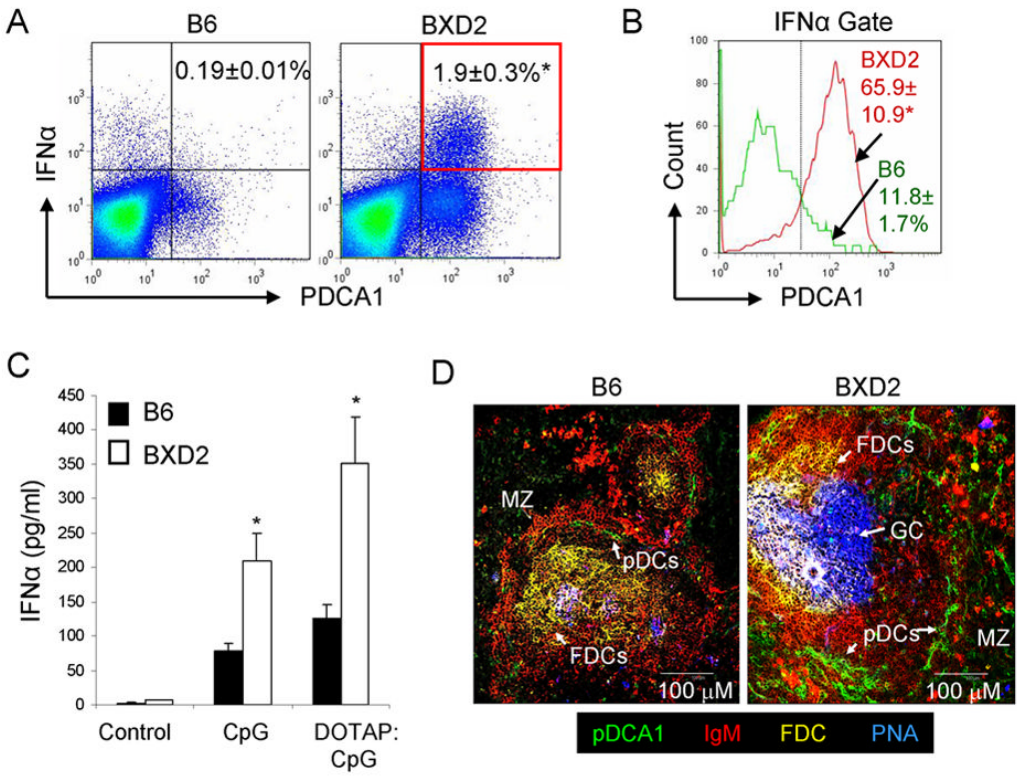

FIGURE 1.

Increased type I IFN-producing pDCs in the spleens of BXD2 mice. ***A***, Flow cytometry was performed on B6 and BXD2 spleen cells labeled with anti-IFNα and anti-PDCA1 antibodies. Means ± SEM. (n=6); * $P < 0.05$ compared with B6 mice. ***B***, Gating on IFNα$^+$ cells, the frequencies of BXD2 and B6 PDCA1$^+$ cells were determined. Means ± SEM. (n=6); * $P < 0.05$ compared with B6 mice. ***C***, ELISA analysis of the levels of IFNα produced by unstimulated, CpG, or DOTAP complexed to CpG (DOTAP:CpG) stimulated pDCs isolated from the spleens of B6 (black bars) and BXD2 mice (white bars). pDCs were enriched and cultured *in vitro* for 24 hours with the indicated stimulations. Means ± SEM (n=6); * $P < 0.05$ compared with B6 mice. ***D***, Confocal imaging analysis of spleen sections taken from B6 and BXD2 mice that were stained with fluorescent conjugated anti-PDCA1, anti-IgM, anti-CD35 (FDC), and PNA-biotin followed by an Alexa 350-conjugated secondary antibody as described in the Materials and Methods. Data are representative of three independent experiments.

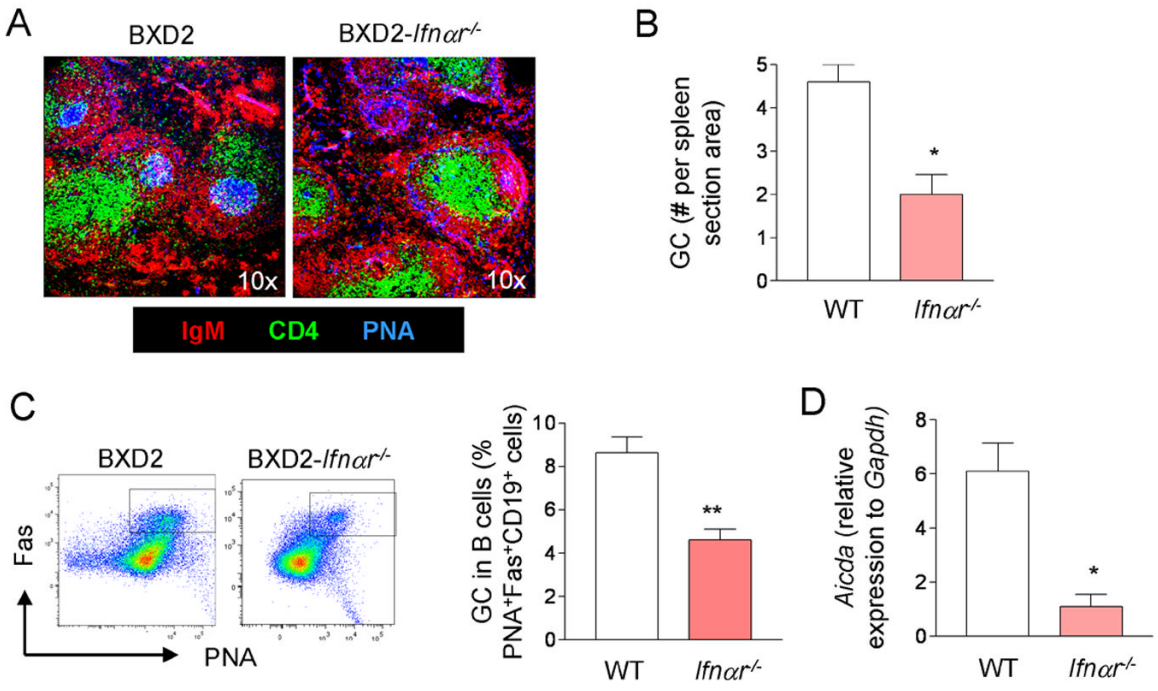

FIGURE 2.

Type I IFN receptor deletion diminishes GC responses in BXD2 mice. ***A***, Confocal imaging analysis of spleen sections from 3-mo-old BXD2 and BXD2-*Ifnar*$^{-/-}$ mice stained with anti-IgM (red), anti-CD4 (green) antibodies, and PNA (blue) (original objective lens magnification ×10). ***B***, The quantitative counts of PNA^{+} GCs per visual field for wild-type BXD2 (WT) and BXD2-*Ifnar*$^{-/-}$ *mice*. Means ± SEM (n=5); **P* < 0.05 compared with wild-type BXD2 mice. ***C***, Flow cytometry analysis of the percentage of PNA^{+}Fas^{+} B220^{+} B cells in the spleens of 6-mo-old BXD2 and BXD2-*Ifnar*$^{-/-}$ mice. Representative FACS plots are shown in left panels, and quantitative bar graph for wild-type BXD2 (WT) and BXD2-*Ifnar*$^{-/-}$ mice is shown in the right. Means ± SEM (n=6); ***P* < 0.01 compared with wild-type BXD2 mice. ***D*,** QRT-PCR analysis for transcript levels of *Aicda* in enriched B cells from the spleens of 3-mo-old wild-type BXD2 (WT) and BXD2-*Ifnar*$^{-/-}$ mice. Means ± SEM (n=6); **P* < 0.05 compared with wild-type BXD2 mice.

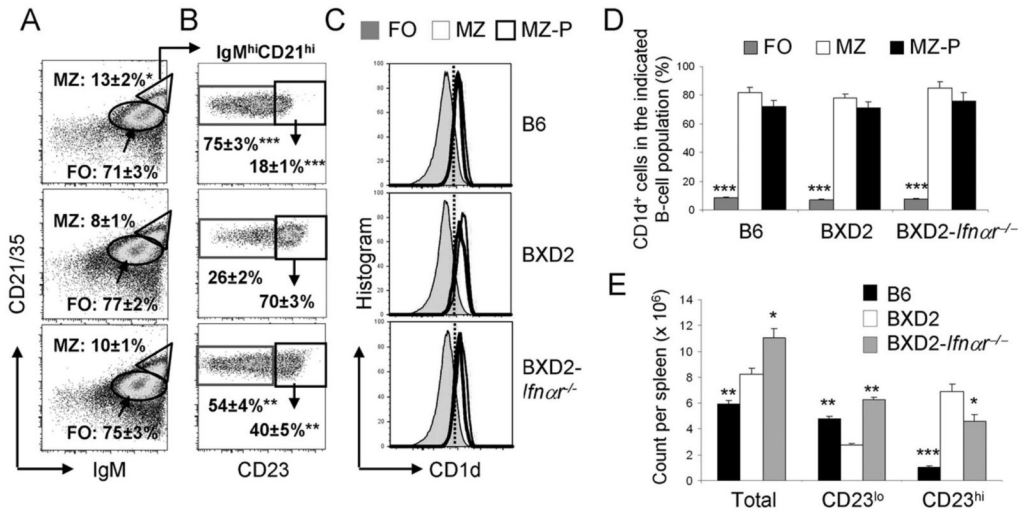

FIGURE 3.

Increased MZ-P B cells in BXD2 mice. Single cell suspensions were prepared from the spleens of 3-mo-old B6, BXD2, and BXD2-*Ifnαr*$^{-/-}$ mice. ***A***, Flow cytometry analysis of the percent of FO (oval) and total MZ (triangle) B (CD19^{+}) cells in the indicated mouse strain. Means ± SEM (n=6); * $P < 0.05$ compared with wild-type BXD2 mice. ***B***, Gated within the total IgM^{hi}CD21^{hi} B cells, cells were further gated as CD23$^{null+lo}$ MZ or CD23^{hi} MZ-P B cells (rectangle gated cells). Means ± SEM (n=6); ** $P < 0.01$, or *** $P < 0.005$ compared with the same population of cells from wild-type BXD2 mice. ***C***, Gating for CD23^{hi}IgM^{hi}CD21^{hi} MZ-P, CD23$^{null+lo}$IgM^{hi}CD21^{hi} MZ, and FO B cell populations, cell populations were further gated for the percentage of cells expressing CD1d. ***D***, Bar graph showing the average of CD1d expression in FO, MZ and MZ-P B cells. Means ± SEM (n=6); *** $P < 0.005$ compared with MZ or MZ-P B cells. ***E,*** Absolute counts of splenic IgM^{hi}CD21^{hi} (Total), MZ (CD23^{lo}), and MZ-P (CD23^{hi}) B cells. Means ± SEM (n=6); * $P < 0.05$, ** $P < 0.01$, *** $P < 0.005$ compared with the same population of cells from wild-type BXD2 mice.

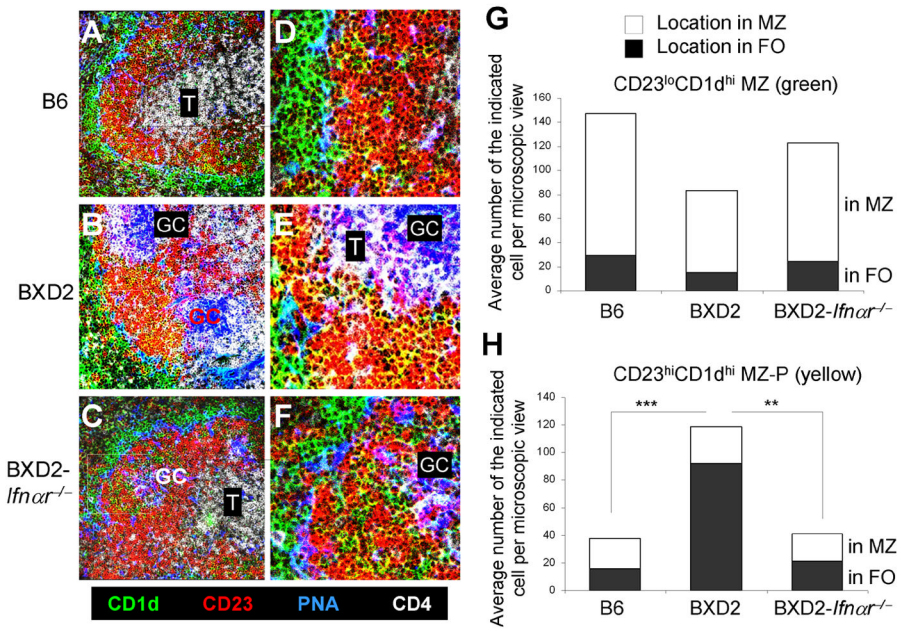

FIGURE 4.

Increased follicular concentration of MZ-P B cell aggregation in proximity to GCs in type I IFN-competent BXD2 mice. ***A–C,*** Confocal imaging analysis of spleen sections from B6, BXD2, and BXD2-*Ifnαr*$^{-/-}$ mice stained with fluorescent-conjugated anti-CD1d (green), anti-CD23 (red), PNA (blue; GC), and anti-CD4 (white; T) (original objective lens magnification ×10). ***D–F,*** Confocal imaging analysis at 40× magnification of the distribution of CD1d^{hi}CD23^{hi} (yellow) MZ-P B cells in the indicated rectangle area from panels A to C (original objective lens magnification ×40). ***G,*** Quantitative counts of CD23^{lo}CD1d^{hi} (green) B cells in the anatomic location of MZ and FO, and ***H,*** Quantitative counts of CD23^{hi}CD1d^{hi} (yellow) B cells in the anatomic location of MZ and FO; Means ± SEM (n=4–7); A chi-square test comparing percentages of each B cell population in the FO, ** $P < 0.01$, *** $P < 0.005$ compared with BXD2 mice.

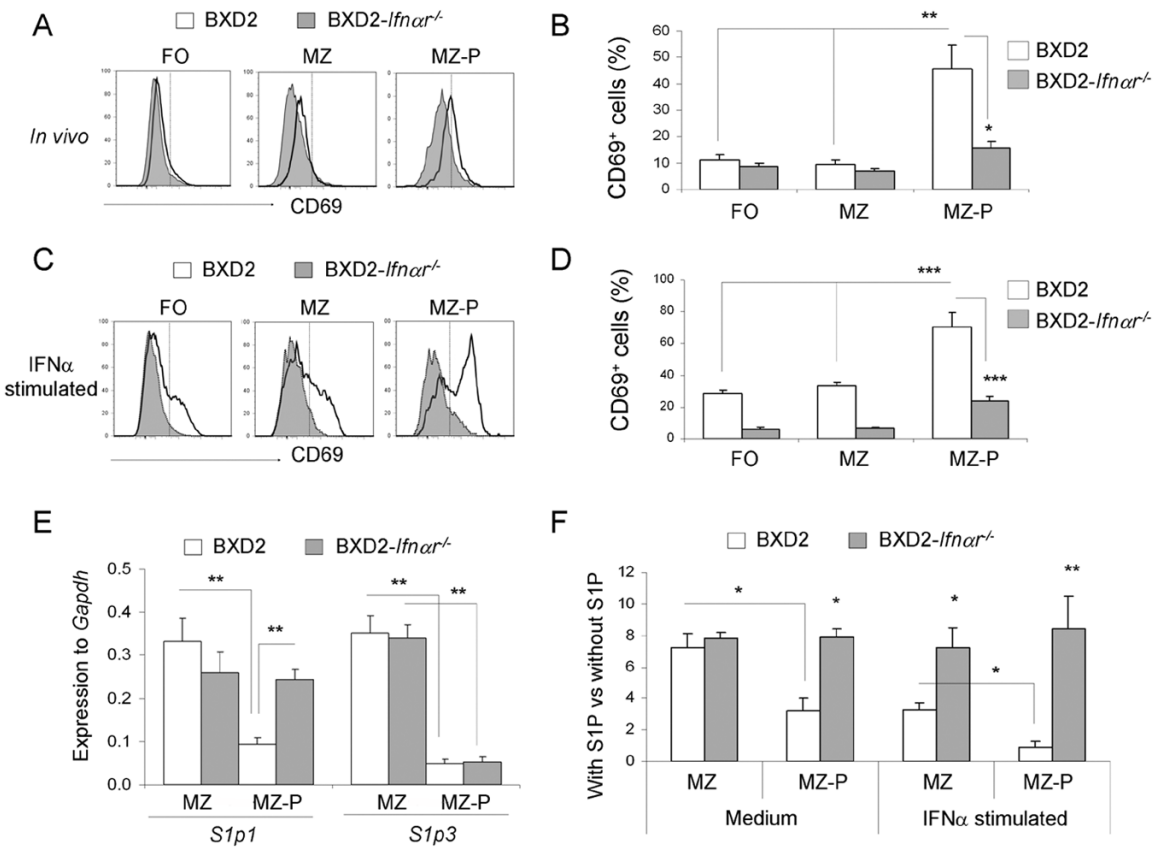

FIGURE 5.

Increased sensitivity in MZ-P B cells to type I IFN-induced CD69/S1P$_1$ signaling. ***A–D***, Flow cytometry analysis of the percent of CD69$^+$ FO, MZ, and MZ-P subpopulations of B cells in the spleens of 2-mo-old BXD2 and BXD2-*Ifnαr*$^{-/-}$ mice. Single cell suspensions from the spleens of mice were ***A***, freshly isolated, or ***C***, stimulated with IFNα (20 ng/ml) for 12 hours, and the expression of CD69 on the indicated populations of B cells was determined. One representative experiment of a total of four samples per group is shown. ***B*** and ***D***, Bar graph showing the expression of CD69 on each population of B cells either *in vivo* (**B**) or after stimulated with IFNα *in vitro* (**D**). Means ± SEM (n=4); * P <0.05, ** P < 0.01, or *** P <0.005 compared with wild-type BXD2 mice or compared with non-MZ-P B cell population. ***E***, QRT-PCR analysis of *S1p1* and *S1p3* transcripts in FACS sorted MZ and MZ-P B cells from the spleens of the indicated strain of mice. Means ± SEM (n=4); ** P < 0.01 compared with wild-type BXD2 mice, or compared with CD23^{lo} MZ B cell population. ***F***, Chemotactic response on B cells from 3-mo-old BXD2 and BXD2-*Ifnαr*$^{-/-}$ mice was analyzed using a Transwell migration chamber with S1P (20 nM) or culture medium loaded in the bottom chamber. Cells were either not stimulated or stimulated with IFNα for 6 hrs prior to carrying out the migration analysis. FACS analysis was carried out to determine the migration response to S1P for the indicated populations of B cells. Means ± SEM (n=6); * P <0.05 or ** P <0.01 compared with wild-type BXD2 mice, or compared with CD23^{lo} MZ B cells from BXD2 mice.

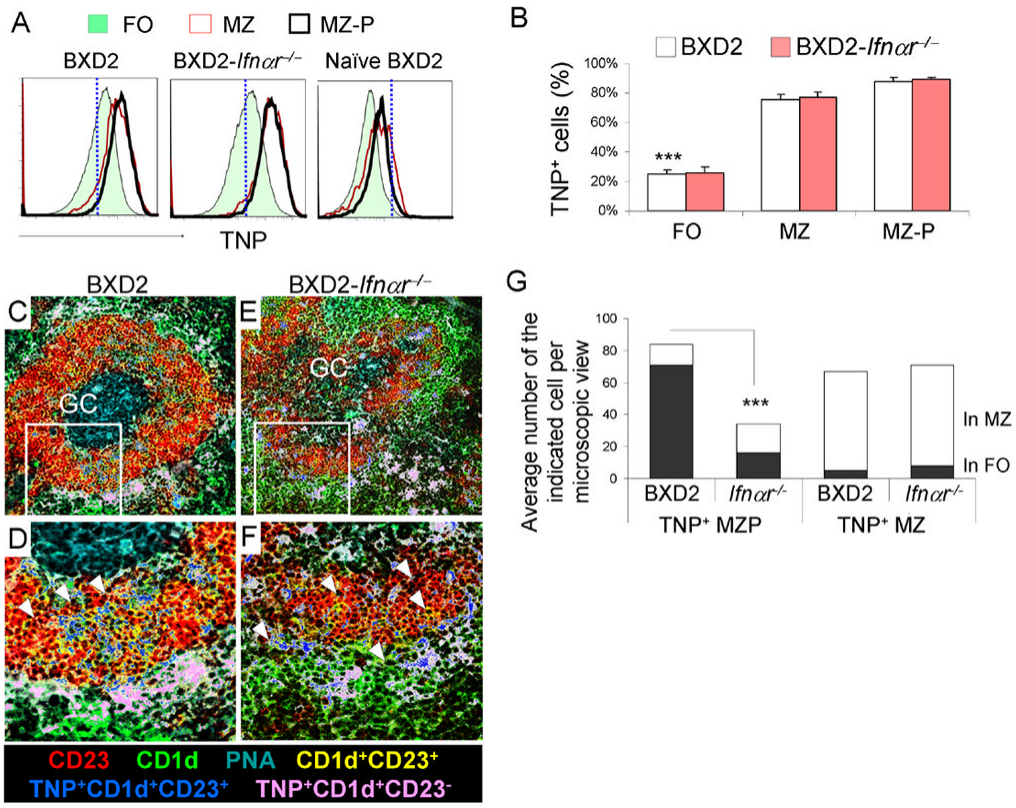

FIGURE 6.

MZ-P B cells deliver Ag rapidly to the interior of FO and GC compared to MZ B cells in type I IFN-competent BXD2 mice. ***A***, Flow cytometry analysis of splenic single-cell suspensions from BXD2 and BXD2-*Ifnαr*$^{-/-}$ mice 1hour after immunizing with TNP-Ficoll compared to naïve BXD2 mice. Gating on FO, MZ, MZ-P B cell subpopulations, TNP^{+} cells were determined. ***B***, Bar graph showing the expression of TNP on each population of B cells. Means ± SEM (n=4); *** P <0.005 compared FO with MP or MZ-P B cells from either BXD2 or BXD2-*Ifnαr*$^{-/-}$ mice. ***C–F***, Representative images taken using a confocal microscope showing the location of TNP^{+} MZ (CD21^{+}CD23^{-})(pseudo-colored to pink) and TNP^{+} MZ-P (CD21^{+}CD23^{+})(pseudo-colored to blue) in the spleens of TNP-Ficoll injected BXD2 (***C***) and BXD2-*Ifnαr*$^{-/-}$ mice (***E***). Selected areas were further enlarged to illustrate the inner migration of TNP^{+} MZ-P B cells towards a spontaneous GC in the spleen of the representative BXD2 mouse (***D***) and lack of such behavior in the spleen of the representative BXD2-*Ifnαr*$^{-/-}$ mouse (***F***) (original objective lens magnification ×10 for C and E; ×40 for D and F). ***G,*** Quantitative counts of TNP^{+} CD23^{hi}CD1d^{hi} (light blue) and TNP^{+} CD23^{lo}CD1d^{hi} (pink) B cells in the anatomic location of MZ and FO; A chi-square test comparing percentages of the blue cells in the FO between BXD2 and BXD2-*Ifnαr*$^{-/-}$ mice (*** P < 0.005; results are the average number, n=12 randomly chosen follicles of the indicated cell per microscopic view from spleen sections from each strain).